Unconventional ballooning structures for toroidal drift waves

Hua-sheng Xie and Yong Xiao

Citation: Physics of Plasmas **22**, 090703 (2015); doi: 10.1063/1.4931072
View online: http://dx.doi.org/10.1063/1.4931072
View Table of Contents: http://scitation.aip.org/content/aip/journal/pop/22/9?ver=pdfcov
Published by the AIP Publishing

Unconventional ballooning structures for toroidal drift waves

Hua-sheng Xie[a] and Yong Xiao[b]
Institute for Fusion Theory and Simulation, Department of Physics, Zhejiang University, Hangzhou 310027, People's Republic of China

(Received 3 August 2015; accepted 1 September 2015; published online 14 September 2015)

With strong gradients in the pedestal of high confinement mode (H-mode) fusion plasmas, gyrokinetic simulations are carried out for the trapped electron and ion temperature gradient modes. A broad class of unconventional mode structures is found to localize at arbitrary poloidal positions or with multiple peaks. It is found that these unconventional ballooning structures are associated with different eigen states for the most unstable mode. At weak gradient (low confinement mode or L-mode), the most unstable mode is usually in the ground eigen state, which corresponds to a conventional ballooning mode structure peaking in the outboard mid-plane of tokamaks. However, at strong gradient (H-mode), the most unstable mode is usually not the ground eigen state and the ballooning mode structure becomes unconventional. This result implies that the pedestal of H-mode could have better confinement than L-mode. © *2015 AIP Publishing LLC*.
[http://dx.doi.org/10.1063/1.4931072]

Although numerous theoretical models have been suggested,[1] a yet unexplained phenomenon in tokamak fusion plasmas is the transition of low (L) to high (H) confinement states, where H-mode[2] has significant better confinement property than that of the L-mode. Understanding of the H-mode physics is not only important to make controlled fusion more feasible but also that the existence of and transitions among multi-equilibrium states are important fields of nonlinear physics in laboratory and the Universe. Drift wave turbulence is one of the major causes that leads to the anomalous transport widely observed in fusion and space plasmas.[3,4] In order to control the turbulent transport, it is crucial to understand the underlying transport mechanism, which may vary for different types of instability that drive the turbulence. The correlation time and length are found to be closely related to the mode structure of the turbulence.[5] Therefore, the mode structure of the turbulence has a significant effect on the transport level.[6]

In this letter, we show that the linear properties of two major types of electrostatic micro-instabilities,[3] namely, the trapped electron mode (TEM) and ion temperature gradient (ITG) mode, are completely different in the H-mode (strong gradient) and L-mode (weak gradient) stages. With the conventional weak gradient, the mode structures for drift wave instabilities such as the ITG and TEM are of ballooning type, peaking at the outboard mid-plane of the tokamak (cf. Refs. 7 and 8). This type of solution has been intensively studied using the ballooning-representation[9,10] by reducing one two-dimensional (2D) real space eigen mode equation for the drift waves to two one-dimensional (1D) ballooning space eigen mode equations. For the 2D case, we solve the eigen equation in the poloidal plane. For the 1D case, we solve the eigen equation in the parallel direction. The most unstable solutions in the ballooning space found in the past have usually the ballooning-angle parameter $\vartheta_k = 0$,[11] which corresponds to the solution localized at the outside mid-plane, i.e., $\theta_p = 0$ in our notation, where θ_p is defined as the local peaking poloidal angle for the mode structure. For this reason, many local eigenvalue codes such as HD7[12] assume implicitly $\vartheta_k = 0$. The unconventional eigen modes with $\theta_p \neq 0$ have been recently discovered in the strong gradient parameter regime. Typically, $|\theta_p| \simeq$ or $< \pi/2$ have been shown to exist.[7,8,13,14] In this work, we find the most general unconventional eigen mode structures from first principle gyrokinetic simulations. The underlying physics is also explained and it has important implications for turbulent transport.

We first obtain linear electrostatic results from global gyrokinetic particle simulation using the GTC code[15,16] with single toroidal mode number n. The simulation parameters and profiles are similar to that of the recent H-mode experiments of the HL-2A tokamak:[17] toroidal magnetic field $B_0 = 1.35$ T, minor radius $a = 40$ cm, major radius $R_0 = 165$ cm, safety factor $q = 2.5$–3.0, magnetic shear $s = 0.3$–1.0, and $R_0/L_n = 80$–160 with $T_e(r) = T_i(r)$ and $n_e(r) = n_i(r)$. $L_n \equiv -(1/n)(dn/dr)$ and $L_T \equiv -(1/T)(dT/dr)$ are density and temperature gradient scale length. Typical electron temperature (also density) profiles used in this letter are shown in Fig. 1. We start with $\eta = L_n/L_T = 1.0$ for simplicity. Collisions are included in some cases but shown little influence to the general results. Under these parameters, no instability or only weakly unstable mode can be found when the electrons are adiabatical. Thus, the major instability for these simulation parameters is the trapped electron mode.

These TEM simulations show that both conventional and unconventional ballooning mode structures can exist for various gradients and toroidal mode numbers ($n = 5$–30), as shown by Fig. 2. In these sub-figures, q profiles are similar. For Figs. 2(b)–2(i), the global density (also temperature) profiles and toroidal mode numbers are not the same but all are under strong gradient. The novel features include: (a) the mode can have anti-ballooning structure (i.e., $|\theta_p| > \pi/2$, e.g., Fig. 2(g)); (b) the mode can have multiple peaks (e.g., Fig. 2(b)). Considering that the trapped particles are mainly

[a]Email: huashengxie@gmail.com
[b]Author to whom correspondence should be addressed. Electronic mail: yxiao@zju.edu.cn

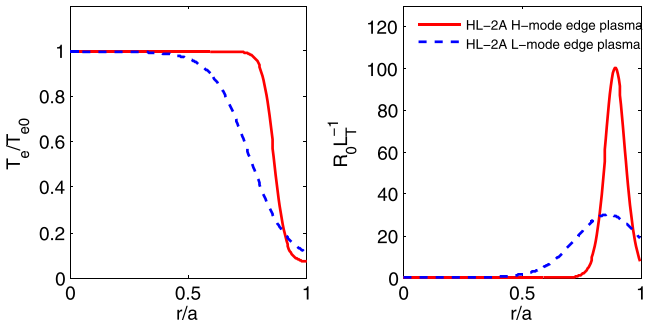

FIG. 1. Typical electron temperature (also density) profiles used in this letter. HL-2A L-mode edge plasma profile is weak gradient $R_0L_T^{-1} < 40$. HL-2A H-mode edge plasma profile is strong gradient $R_0L_T^{-1} > 80$.

located at the low magnetic field side, i.e., the outboard side, the anti-ballooning structures of TEM are not expected. The 3D mode structure of the electrostatic potential can be represented by the Fourier series $\delta\phi(r,\theta,\zeta) = e^{in\zeta}\sum_m \delta\phi_m(r)e^{-im\theta}$, where m is poloidal mode number. To explore the formation of these different eigenmode structures, we compute the $\delta\phi_m(r)$ for several typical conventional and unconventional mode structures, as shown in Fig. 3. For the conventional ballooning structure, the poloidal eigen modes $\delta\phi_m(r)$ are almost radially symmetric (Gaussian-like) and positive in amplitude. And, $\delta\phi_m$ has a large overlap with $\delta\phi_{m+1}$, i.e., $\delta\phi_m \simeq \delta\phi_{m+1}$. However, for the unconventional structures, the poloidal eigen modes $\delta\phi_m(r)$ can be radially either symmetric or asymmetric, and the amplitude for each symmetric mode can be either positive or negative, as shown

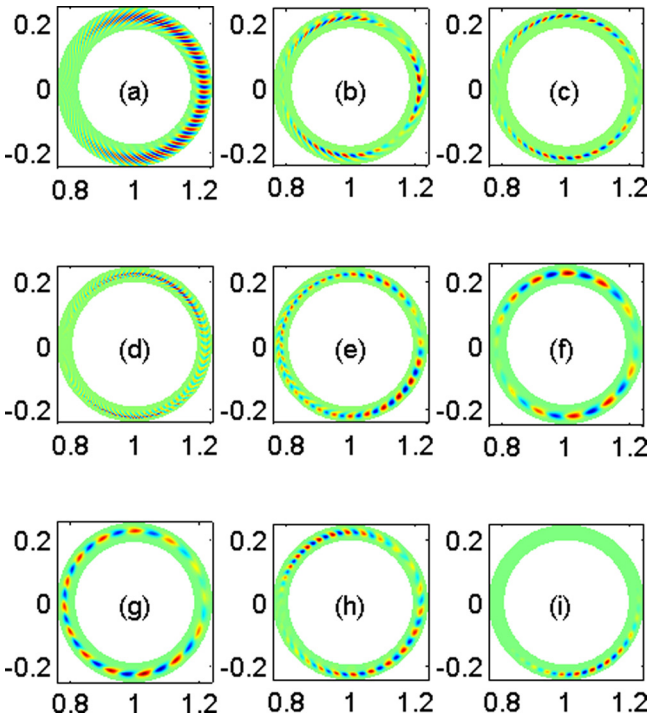

FIG. 2. Conventional (a) and unconventional (b)–(i) 2D ballooning structures of electrostatic potential in (X,Z) plane for TEM observed in GTC simulation, where (a) uses HL-2A tokamak edge weak gradient L-mode plasma parameter ($R_0L_n^{-1} < 40$) and (b)–(i) use edge strong gradient H-mode parameters ($R_0L_n^{-1} > 80$). Collisions are only included in (e) and (g).

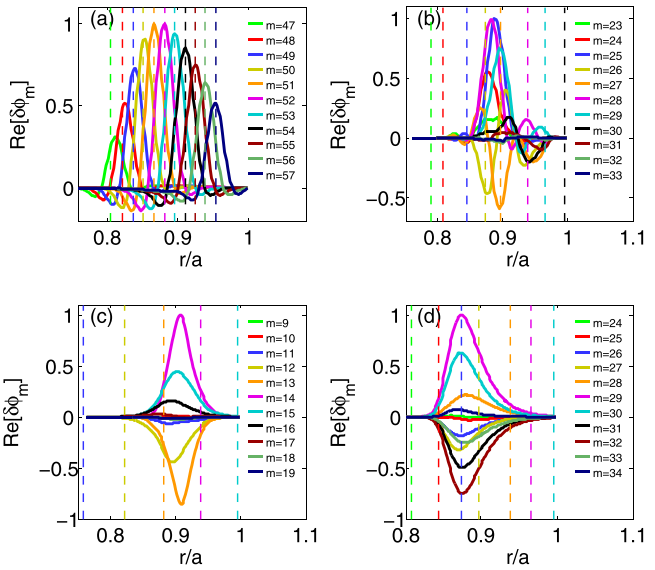

FIG. 3. The real part of Fourier $\delta\phi_m(r)$ for conventional and unconventional mode structures. The corresponding poloidal cross section mode structures of (a)–(d) ($n = 20$, 10, 5, 10, respectively) are taken from Figs. 2(a), 2(b), 2(g), and 2(i), respectively. The dashed lines are corresponding rational surface positions r_s, where $nq(r_s) = m$.

by Figs. 2(b)–2(d). Under stronger gradients, the radial peaking position of $\delta\phi_m(r)$ is also not at the corresponding rational surface position r_s any more, where $nq(r_s) = m$.

Next, we consider ITG mode by reducing the density gradient to $R_0/L_n < 40$ and keeping the other parameters the same as those for the TEM case, e.g., $R_0/L_T > 80$ and thus $\eta_i = L_n/L_T > 2.0$. To completely exclude the contribution of the kinetic electrons, we use adiabatic electrons in the simulations. It is found that the preceding unconventional mode structures still exist and exhibit even more structural variations. For example, the anti-ballooning structure is found for this ITG simulation, as is shown in Figs. 4(a) and 4(b). Actually, the mode structure with global profiles and multi modes coexisting in the initial value simulation can be even more complicated. For example, two modes with similar growth rates can be excited in different radial locations, as shown in Figs. 4(c) and 4(d). Multi modes coexist with close peaking positions in the initial value simulation can also lead to $\theta_p = \theta_p(t)$, i.e., rotate poloidally with time. Thus, the unconventional mode structures are not limited to TEM and can be common for drift waves.

These unconventional linear behaviors can be understood from the following eigenmode analysis. We start with the ITG eigen mode equation[8,10]

$$\left[\rho_i^2\frac{\partial^2}{\partial x^2} - \frac{\sigma^2}{\omega^2}\left(\frac{\partial}{\partial\theta} + ik_\theta sx\right)^2 - \frac{2\epsilon_n}{\omega}\left(\cos\theta + \frac{i\sin\theta}{k_\theta}\frac{\partial}{\partial x}\right) - \frac{\omega-1}{\omega+\eta_s} - k_\theta^2\rho_i^2\right]\delta\phi(x,\theta) = 0, \quad (1)$$

where $\sigma = \epsilon_n/(qk_\theta\rho_i)$, $\epsilon_n = L_n/R_0$, $\eta_s = 1 + \eta_i$, $x = r - r_s$, r_s is the rational surface, $\omega = \omega_r + i\gamma$ is the complex mode frequency normalized by the electron diamagnetic frequency, and the poloidal wave number $k_\theta = nq/r$. Eq. (1) can be derived from the gyrokinetic theory with adiabatic electron

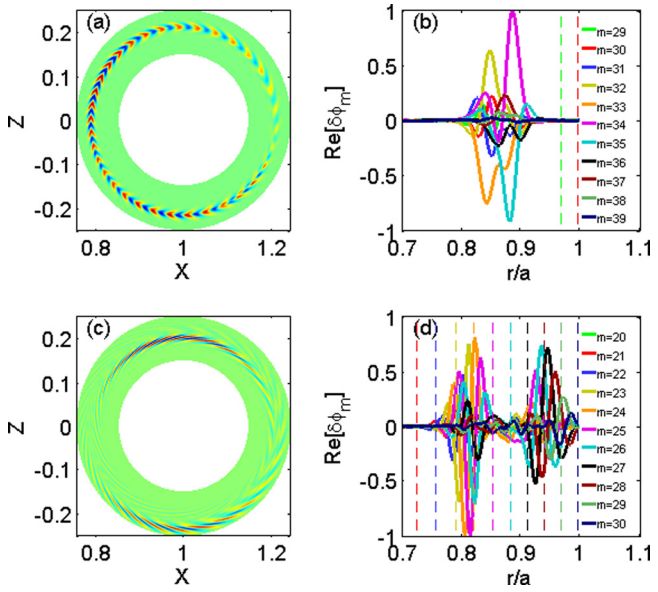

FIG. 4. Unconventional ITG ($n=10$) mode structures in GTC. (a) and (b) Anti-ballooning structure. (c) and (d) Two modes co-exist (or, one mode with two radius peaks) at different radius positions. One has $\theta_p \simeq \pi/2$ and another has $\theta_p \simeq -\pi/2$.

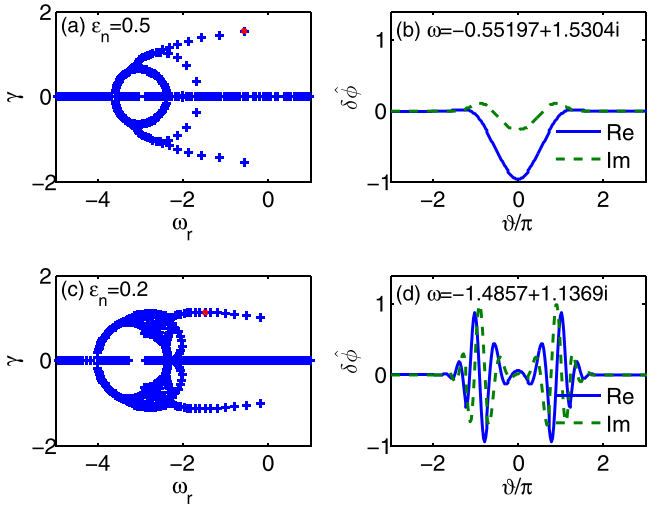

FIG. 5. In Eq. (2), series of solutions exist. For weak gradient ($\epsilon_n=0.5$), the most unstable solution (red "x") is the ground state (a) and (b), which is the conventional ballooning structure. For strong gradient ($\epsilon_n=0.2$), the most unstable solution (red "x") is not the ground state (c) and (d), which represents the unconventional ballooning structure.

assumption. The corresponding 1D eigen mode equation in the ballooning space is

$$\left\{\frac{\sigma^2}{\omega^2}\frac{d^2}{d\vartheta^2}+k_\theta^2\rho_i^2\left[1+s^2(\vartheta-\vartheta_k)^2\right]+\frac{2\epsilon_n}{\omega}\left[\cos\vartheta+s(\vartheta-\vartheta_k)\sin\vartheta\right]+\frac{\omega-1}{\omega+\eta_s}\right\}\delta\hat{\phi}(\vartheta,\vartheta_k)=0, \tag{2}$$

where ϑ_k is the ballooning-angle parameter, which represents an as yet undetermined radial wavenumber.[10] The relation between the ballooning space electrostatic potential $\delta\hat{\phi}(\vartheta,\vartheta_k)$ and real space $\delta\phi(x,\theta)$ can be found in Refs. 8 and 10. Using the Fourier basis $\delta\phi(x,\theta)=\sum_m \delta\phi_m e^{-im\theta}$, Eq. (1) can be rewritten as the 2D eigenmode equation

$$k_\theta^2\rho_i^2 s^2\frac{\partial^2\delta\phi_m}{\partial z^2}+\frac{\sigma^2}{\omega^2}(z-m)^2\delta\phi_m-\frac{\epsilon_n}{\omega}\left[\left(1-s\frac{\partial}{\partial z}\right)\delta\phi_{m-1}+\left(1+s\frac{\partial}{\partial z}\right)\delta\phi_{m+1}\right]-\left(\frac{\omega-1}{\omega+\eta_s}+k_\theta^2\rho_i^2\right)\delta\phi_m=0, \tag{3}$$

where $z=k_\theta s x$. To solve the eigenvalue problem of Eq. (3), only a few number of m modes need to be kept for the solution to reach convergence.

With suitable approximations (cf. Ref. 22), both Eqs. (2) and (3) can be reduced to the Weber equation $u''+(bx^2+a)u=0$ (here, the argument x is ϑ and z for Eqs. (2) and (3), respectively), which has solutions with the eigenvalues $a(\omega)=i(2l+1)\sqrt{b(\omega)}$ and eigenfunctions $u(x)=H_l(i\sqrt{b}x)e^{-ibx^2/2}$, where H_l is l-th Hermite polynomial and $l=0, 1, 2,\ldots$, which represent a series eigenstates. With the original equations, i.e., Eqs. (2) and (3), which can only be solved numerically, the eigenstates take a more complicated form.

Eqs. (2) and (3) can be solved numerically by transforming it to a matrix eigenvalue problem as $\omega^3\boldsymbol{M}_3\boldsymbol{X}+\omega^2\boldsymbol{M}_2\boldsymbol{X}+\omega\boldsymbol{M}_1\boldsymbol{X}+\boldsymbol{M}_0\boldsymbol{X}=0$, with X is the discrete representation of the electrostatic potential. We use finite difference to discretize the system, which yields sparse matrices for $\boldsymbol{M_i}$ ($i=0, 1, 2, 3$). Using the companion matrix method, the nonlinear eigenvalue problem can be transformed to a standard eigenvalue problem as $\boldsymbol{AY}=\omega\boldsymbol{BY}$, where $\boldsymbol{Y}=[\boldsymbol{X}_1,\boldsymbol{X}_2,\boldsymbol{X}_3]\equiv[\boldsymbol{X},\omega\boldsymbol{X},\omega^2\boldsymbol{X}]$, $\boldsymbol{A}=[\boldsymbol{O},\boldsymbol{I},\boldsymbol{O};\boldsymbol{O},\boldsymbol{O},\boldsymbol{I};-\boldsymbol{M}_0,-\boldsymbol{M}_1,-\boldsymbol{M}_2]$, $\boldsymbol{B}=[\boldsymbol{I},\boldsymbol{O},\boldsymbol{O};\boldsymbol{O},\boldsymbol{I},\boldsymbol{O};\boldsymbol{O},\boldsymbol{O},\boldsymbol{M}_3]$, and $\boldsymbol{I}$ and $\boldsymbol{O}$ are unit and null matrix, respectively. Thus, all the solutions of this eigen system can be obtained (cf. Ref. 18 for details of similar treatment). The advantage of this method is that it can show the complete set solutions of the discrete eigen system and help us to understand the distribution of eigenvalues in the complex plane. The solution in Refs. 7 and 8 using iterative solver is actually just one of the solutions obtained here and may not be the most unstable or most important, which depends heavily on the initial guess. This companion matrix method has been verified by comparing the numerical solutions with that from the shooting method and the analytical solution for the Weber equation.

By solving Eq. (2) in the 1D ballooning space, the unconventional ballooning structures occur when either the most unstable solution is not the ground eigen state ($l\neq 0$) or the ballooning angle $\vartheta_k\neq 0$. Both of these two conditions can be met in the strong gradient regime. The most unstable solution with $\vartheta_k\neq 0$ has been discussed by others (cf. Refs. 13 and 19). Here, we focus on the unconventional ballooning structure caused by the non-ground eigen state. The following parameters are used to solve Eq. (2): $s=0.8$, $k_\theta\rho_i=0.4$, $q=1.0$, $\eta_s=3.0$, and $\vartheta_k=0$. As is known from the aforementioned analytical analogy, Fig. 5 shows that a series of solutions can exist for Eq. (2), where R/L_T and R/L_n are changed simultaneously to ensure $\eta=L_n/L_T=const.$, and one should also note that the frequency is normalized by the electron diamagnetic frequency. For the weak gradient case

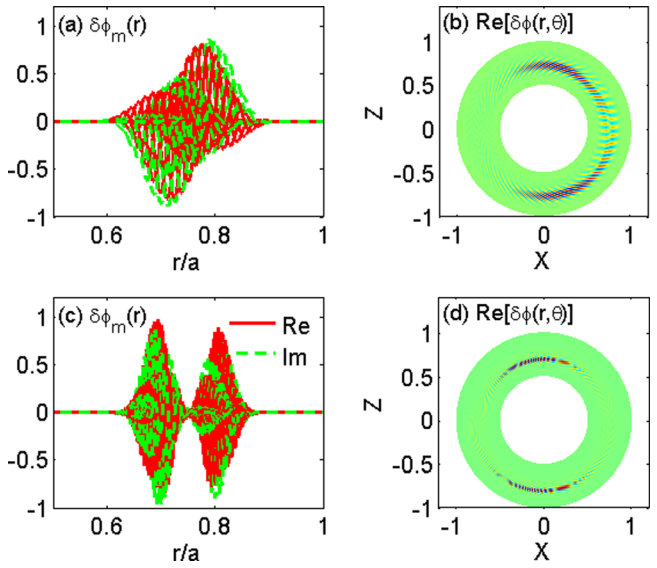

FIG. 6. Typical unconventional mode structures from 2D eigen solution for Eq. (3). (b) is similar to Figs. 2(c) and 2(d), and (c) and (d) are similar to Figs. 4(d) and 4(c).

($\epsilon_n = 0.5$), we find that the most unstable solution is the ground state (Fig. 5(a)), which is the conventional ballooning structure (Fig. 5(b)). For the strong gradient case ($\epsilon_n = 0.2$), the most unstable solution is not the ground state (Figs. 5(c) and 5(d)), which corresponds to the unconventional ballooning structure. More detailed analysis[21] of Eq. (2) for present discussion of the unconventional mode structure can be obtained by extension of Refs. 20 and 22.

We have demonstrated that, with strong gradient, the most unstable solution can shift from ground state to other non-ground states, which is analogous to the quantum jump between energy levels. Physically, the jump behavior can be understood from the effective potential.[20] The jump happens from one potential well to another, which leads to different energy levels. It is not transparent that the non-ground eigen state in the 1D ballooning space corresponds to the unconventional mode structure in the 2D poloidal plane. Next, we confirm this link by showing that the non-ground 2D eigen state solved from Eq. (3) can form the unconventional mode structures observed in the preceding gyrokinetic simulation. The solutions in Refs. 7, 8, and 13 are just weak asymmetric solutions of our series solutions. Almost all the mode structures in Figs. 2 and 4 have also been found in the 2D eigen solutions of Eq. (3). Two examples are shown in Fig. 6. Therefore, conventional and unconventional series solutions have been found in both 2D eigen solver and GTC initial simulations. The condition for the jump of the most unstable eigen state to non-ground state is $\epsilon_n < \epsilon_c$, where ϵ_c is a critical gradient parameter which depends on other parameters. In GTC simulations of the HL-2A parameters, the typical critical density (or temperature) gradient value is $R_0/L_n = 40$–120.

The results from the gyrokinetic simulation and eigen mode analysis show that the unconventional mode structures exist mainly in the strong gradient regime or the H-mode. In the weak gradient regime or L-mode, conventional mode structures still prevail. This can indicate different transport behavior between H-mode and L-mode.[23] In the conventional ballooning structure, the neighboring Fourier modes $\delta\phi_m \simeq \delta\phi_{m+1}$, the effective correlation length may be estimated as the width of radial envelope of the modes, say, ΔA. Whereas, in the unconventional ballooning structures, especially for anti-ballooning structure, $\delta\phi_m \simeq -\delta\phi_{m+1}$ can occur, i.e., a 180° phase shift for the neighboring Fourier modes, which can change the effective correlation length to the distance of neighboring mode-rational surfaces Δr_s. Considering that $\Delta r_s \ll \Delta A$, we can expect that the H-mode can have better confinement.

To summarize, a broad class of unconventional ballooning modes is found for electrostatic drift waves (TEM and ITG) by the gyrokinetic simulation, which is shown to be common in the strong gradient regime. These unconventional mode structures are shown to correspond to the non-ground-state solutions of the eigen mode equation. These results may have important implications for the turbulent transport in tokamaks, i.e., the turbulent transport mechanism in the H-mode can be rather different from that in the L-mode, which requires further investigation by self-consistent nonlinear gyrokinetic simulations.

Discussions with L. Chen, H. T. Chen, Z. X. Lu, and Z. Lin are acknowledged. The work was supported by the National Magnetic Confinement Fusion Science Program under Grant Nos. 2015GB110000 and 2013GB111000, the Recruitment Program of Global Youth Experts.

[1]F. Wagner, Plasma Phys. Controlled Fusion **49**, B1 (2007).
[2]F. Wagner *et al.*, Phys. Rev. Lett. **49**, 1408 (1982).
[3]W. Horton, Rev. Mod. Phys. **71**, 735 (1999).
[4]A. Hasegawa, Phys. Fluids **12**, 2642 (1969).
[5]Z. Lin, I. Holod, L. Chen, P. H. Diamond, T. S. Hahm, and S. Ethier, Phys. Rev. Lett. **99**, 265003 (2007).
[6]Y. Xiao, I. Holod, W. Zhang, S. Klasky, and Z. Lin, Phys. Plasmas **17**, 022302 (2010).
[7]T. Xie, Y. Z. Zhang, S. M. Mahajan, and A. K. Wang, Phys. Plasmas **19**, 072105 (2012).
[8]D. Dickinson, C. M. Roach, J. M. Skipp, and H. R. Wilson, Phys. Plasmas **21**, 010702 (2014).
[9]J. W. Connor, R. J. Hastie, and J. B. Taylor, Phys. Rev. Lett. **40**, 396 (1978).
[10]J. W. Connor and J. B. Taylor, Phys. Fluids **30**, 3180 (1987).
[11]G. Rewoldt, W. M. Tang, and M. S. Chance, Phys. Fluids **25**, 480 (1982).
[12]J. Q. Dong, L. Chen, F. Zonca, and G. D. Jian, Phys. Plasmas **11**, 997 (2004).
[13]R. Singh, S. Brunner, R. Ganesh, and F. Jenko, Phys. Plasmas **21**, 032115 (2014).
[14]D. P. Fulton, Z. Lin, I. Holod, and Y. Xiao, Phys. Plasmas **21**, 042110 (2014).
[15]Y. Xiao, I. Holod, Z. Wang, Z. Lin, and T. Zhang, Phys. Plasmas **22**, 022516 (2015).
[16]Z. Lin and T. S. Hahm, Phys. Plasmas **11**, 1099 (2004).
[17]H. S. Xie, Y. Xiao, Z. Lin, and D. F. Kong, "Gyrokinetic simulations of the HL-2A tokamak H-mode edge turbulence. I. Electrostatic physics," (unpublished).
[18]H. S. Xie and Y. Xiao, Phys. Plasmas **22**, 022518 (2015).
[19]Z. X. Lu, Phys. Plasmas **22**, 052118 (2015).
[20]L. Chen and C. Z. Cheng, Phys. Fluids **23**, 2242 (1980).
[21]H. T. Chen, private communication (2015).
[22]W. Horton, D. Choi, and W. M. Tang, Phys. Fluids **24**, 1077 (1981).
[23]L. Chen, private communication (2014).